TUB Summer Research Technical Report

Numerical Simulation of Strake Vortices using Reynolds Stress Models: Longitudinal Vortex behind Delta Wings

Ujjwal Dalmia

Supervisor: M.Sc. Tim Landa

August 2016

Abstract

This study performs numerical simulation of longitudinal vortices generated by slender delta wings using new Reynolds Stress Models for turbulence modeling. Various simulations are performed by varying the sweep angle and angle of attack while recording the vortex characteristics which include maximum vorticity, circulation, core velocity deficit and diameter of vortex. The trends for these values with respect to sweep angle, angle of attack and distance behind the wing are reported. These trends will be used further in the project to design a chine to generate a strake vortex over a commercial high-lift configuration wing.

Table of Contents

Nomenclature

Variable	**Unit**	**Description**
c_{main}	m	Chord length of main wing
c_{Δ}	m	Chord length of Delta wing
ω	s^{-1}	Vorticity
Γ	m^2/s	Circulation
U	m/s	Velocity
U_{∞}	m/s	Freestream Velocity
d_{ω}	m	Diameter of vortex calculated based on vorticity
t_{conv}	s	Convective time step
δ	m	Boundary layer thickness
Re	1	Reynolds number
α	°	Angle of Attack (AOA)

Introduction

Modern aircraft use numerous aerodynamic devices to improve performance and efficiency. Strake vortices are used to improve flow over wings during landing and take-off, in the high-lift configuration. These vortices are generated by delta-shaped chines mounted on the engine nacelle. In the high-lift configuration, while most of the wing has extended flaps and slats, the engine mounting points do not. Without strake vortices, there is flow separation behind the engine mounting points reducing the lift generated by the aircraft. The strake vortex keeps the flow attached thereby improving the efficiency of the wing. The separation of flow and the effect of the strake vortex are discussed by Rudnik and Geyr (2007).

Despite strake vortices being used on most modern aircraft, we do not have a reliable way of simulating strake vortices. Currently strakes are optimized by installing different configuration of strakes on aircraft to find the best position. This can be expensive and the number of test cases would be limited due to the costs. Using numerical simulations significantly reduces the costs and the risk involved in testing and optimizing strake vortices.

The most reliable and accurate numerical simulations are Direct Numerical Simulations (DNS). These directly use the Naiver-Stokes Equations, the governing equations for fluid mechanics. Though highly accurate when performed right, DNS comes with huge computational costs, because DNS resolves every detail of the flow field. This is often not required and in order to reduce computational costs, Reynolds Averaged Naiver Stokes (RANS) equations are used. RANS equations do not resolve all flow phenomenon and use turbulence models to statistically estimate the effect of turbulent flow structures. This project aims to use RANS with Reynolds Stress Models (RSM) to resolve strake vortices. RSM models are a recent development that are closer to the physical world than older models such as Menter-SST. Menter (1993) describes the Menter-SST model, Cecora, Eisfeld, Probst, Crippa & Radespiel (2012) give the details of two different RSM models used in this study, and compare these models to the Menter-SST model. It has been observed that RSM models are better at conserving vortices along the flow, thus having an advantage over Menter-SST models. In this study, the two models are compared to evaluate the difference between the turbulence models.

Strake vortices are generated using delta wings, and this study evaluates the characteristics of the vortex generated by delta wings with varying sweep angles and angles of attack using numerical simulations. The characteristics of strake vortices on aircraft were determined using data from past studies including numerical simulations and PIV data by our partners at the German Aerospace Center (DLR). The objective of this study was to characterize the influence of different parameters on the characteristics of the vortex with the aim to match the strake vortex later in the project.

Approach

Geometry

The geometry used was a sharp leading and trailing edge delta wing with varying sweep angles. The leading edge and trailing edge were shaped by the method described by Subbian

(2016). The final delta wing geometry with 65° sweep can be seen in figure 1. The chord length of the wing is 0.06 m. The dimensions in figure 1 are constant for the other sweep angles.

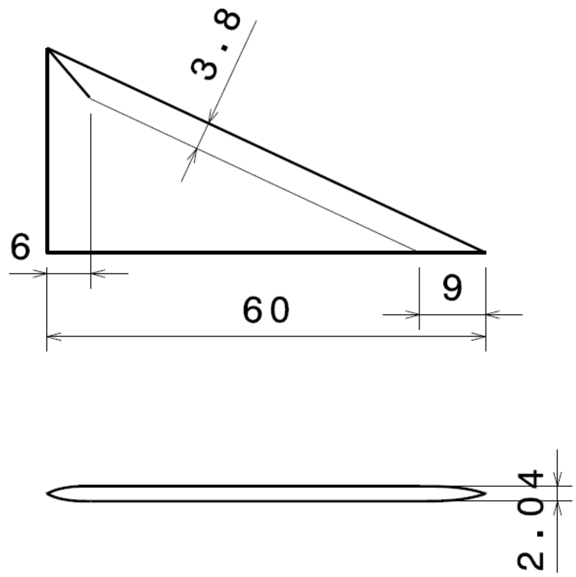

Figure 1: Delta Wing with 65° sweep. (Units: mm)

Grid Generation

The flow domain for the problem was a hemisphere with the diameter of one hundred chord lengths. The mesh used was a hybrid between structured and unstructured meshes. The domain was divided up in sections of structured and unstructured cells as seen in figure 2. The chord lengths referred to in the images are the chord length of the Delta Wing (c_Δ).

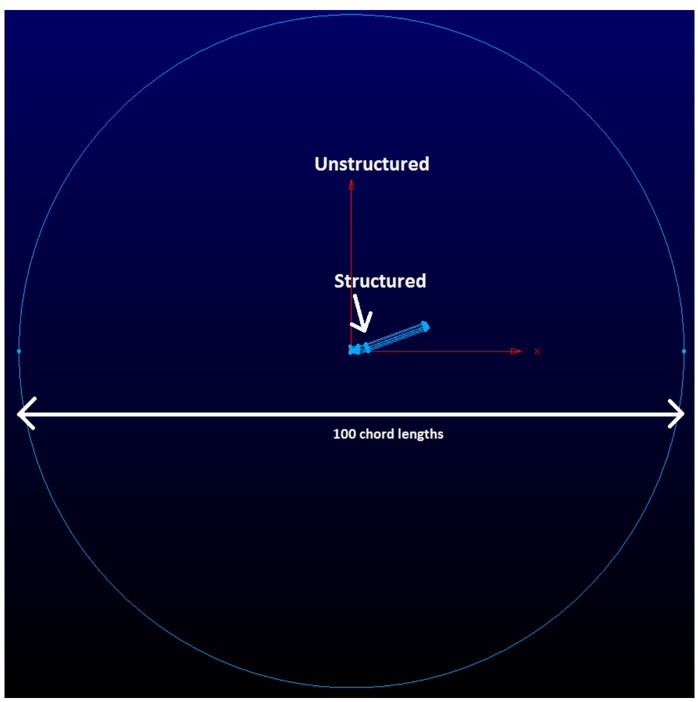

Figure 2: Flow Domain

The surface of the wing was an important part of the grid generation. This determined the grid resolution throughout the domain. The initial surface mesh density was determined based on the analysis of Subbian. This was later refined since the pressure distribution on the wing was not smooth, indicating the mesh was too coarse. The surface mesh for each of the three wings can be seen in figure 3.

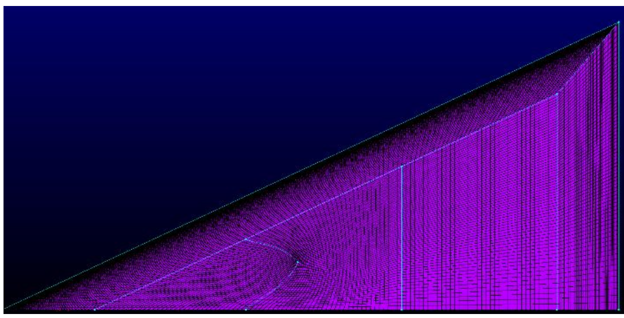

(a) sweep angle 65°

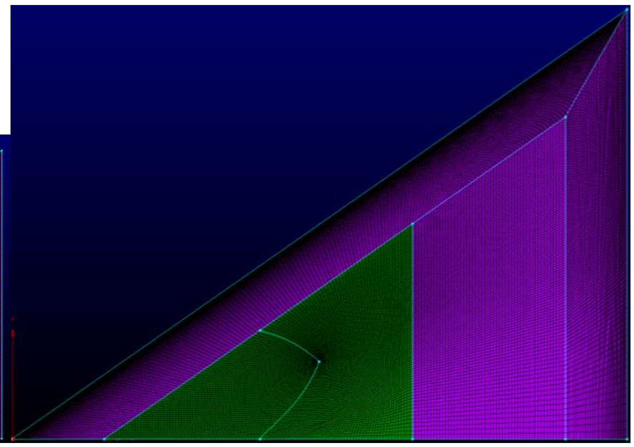

(b) sweep angle 55°

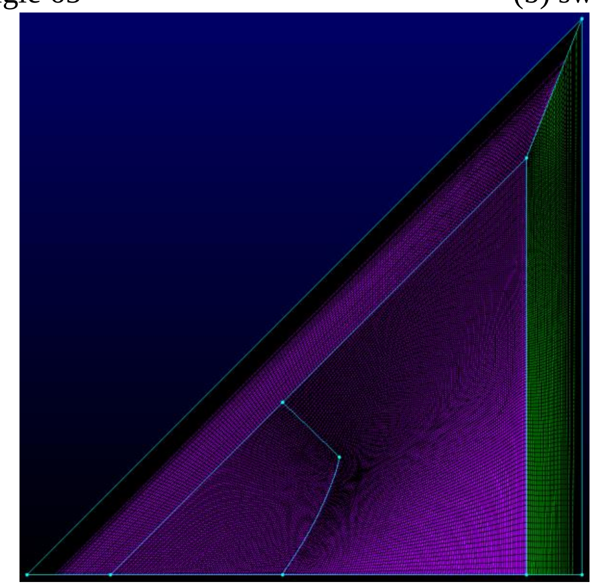

(c) sweep angle 45°

Figure 3: Surface Mesh

The boundary layer is another important part of the flow and can make the difference between an accurate converged solution and an inaccurate or diverged solution. Since the simulations accounted for viscous effects, in order to obtain an accurate solution, the wall distance was set such that the y+ on the most part of the wing was <1. The y+ value over the wing for 65° sweep at 10° angle of attack can be seen in figure 4. The near wall mesh was not modified for the different angles of attack and so the y+ distribution would be similar for other sweep angles and angles of attack. The boundary layer was generated using normal extrusion.

The boundary layer thickness was determined for a turbulent boundary layer using equation 1, where x represents the distance from the leading point on the wing and Re_x is the Reynolds number at that point. The mesh on the upper surface extended above the boundary layer since the vortex would appear in this region.

$$\delta \approx \frac{0.37x}{\sqrt{Re_x{}^{\frac{1}{5}}}}$$

Equation 1: Boundary layer thickness

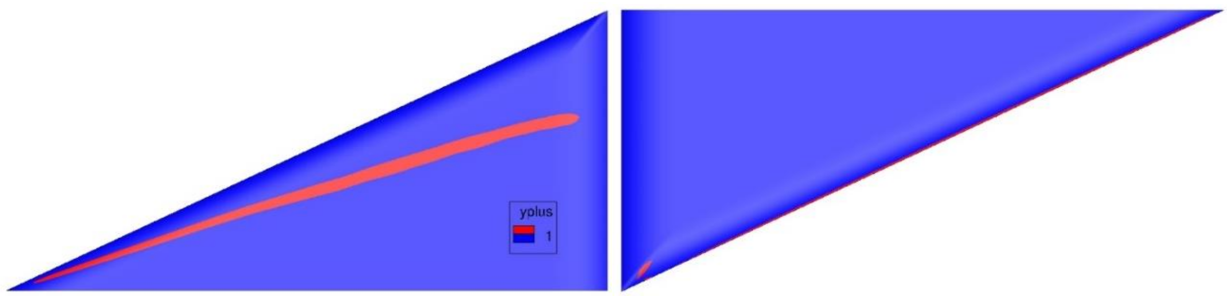

(a) Upper Surface (b) Lower Surface

Figure 4: y+ Distribution

The main objective was to study the vortex characteristics downstream of the delta wing, where the vortex would interact with a high-lift wing. For this purpose structured blocks were used downstream of the wing and this was achieved by translating the downstream boundary layer domain. A separate box of structured cells was created above the boundary layer domain which ensures the vortex stays in the structured region. Structured blocks were used since a structured block with homogenous cells ensures that the vortex can be accurately predicted. As is seen later in this study, unstructured blocks can be used too, but do not produce a smooth vortex.

In order to save computational time, a separate mesh was created for each angle of attack. Doing this eliminated the need for a huge box of structured cells. For each angle of attack, the wake block was sloped up to the angle of attack. The transition from the wing to the wake was made through a rotated section. This arrangement can be seen in figure 5.

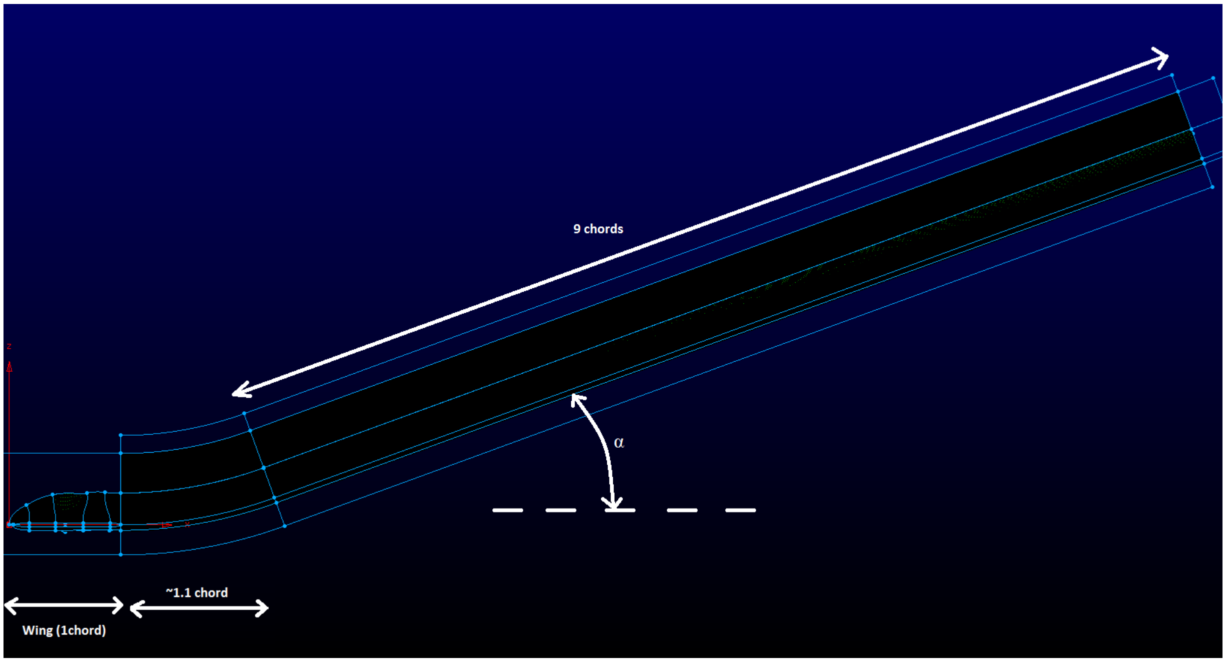

Figure 5: Structured mesh section of the domain

The final grid had ~25 million grid points, with ~17 million structured points and ~12 million unstructured points. The structured region behind the wing, meant to capture the vortex, had ~10 million cells. The exact numbers varied on a case to case basis, but were very close to the reported numbers.

Numerical Simulation

Numerical simulations were performed using the German Space Agency's TAU-Code. The flow conditions can be found in table 1; the parameters file consisting of all the inputs to the code can be found in the appendix. These flow conditions correspond to the planned conditions for the final experiment with a high-lift configuration wing placed downstream.

Table 1: Flow Conditions

Reynold's Number	200,000
Mach Number	0.15
Freestream Velocity (U_∞)	51.48 m/s
Chord Length (c_Δ)	0.06 m
Density	1.1746 kg/m^3
Temperature	293.15 K

The objective of this project is to study strake vortices using RSM models, thus most simulations were run using RSM models. At first simulations were run using the RSM-JHhv2 model. This model requires the user to specify the position of transition from laminar to turbulent flow. Due to the complicated flow around a Delta Wing, the laminar and turbulent flow regions are different from a traditional wing and are documented by Earnshaw & Lawford (1966). Since the user defined transition points did not reflect the real world flow over a Delta Wing, the solution did not converge and kinks were seen in the c_p distribution.

Considering the fact that laminar flow can be considered as flow with negligible turbulence, the flow over the wing was defined as turbulent instead of transition. This did not improve the solution and the kinks persisted. In order to make sure the grid was fine enough, we ran simulations with the tried and tested Menter-SST turbulence model. These simulations did not show any kinks in the c_p distribution, seen in figure 6, proving that the grid was fine enough.

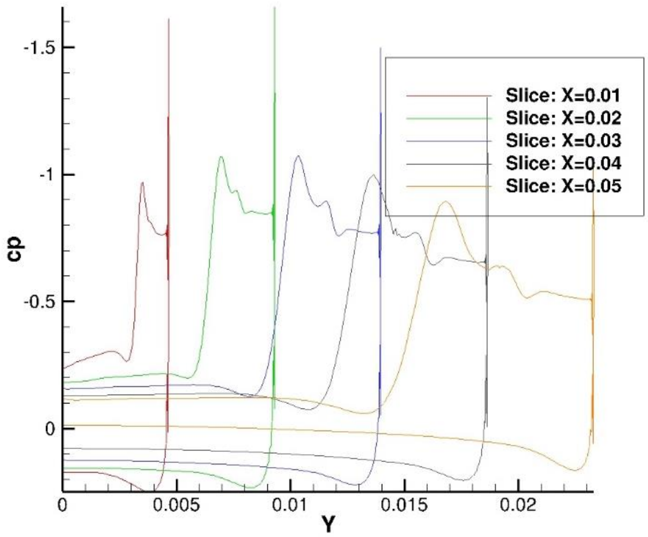

(a) Menter-SST model

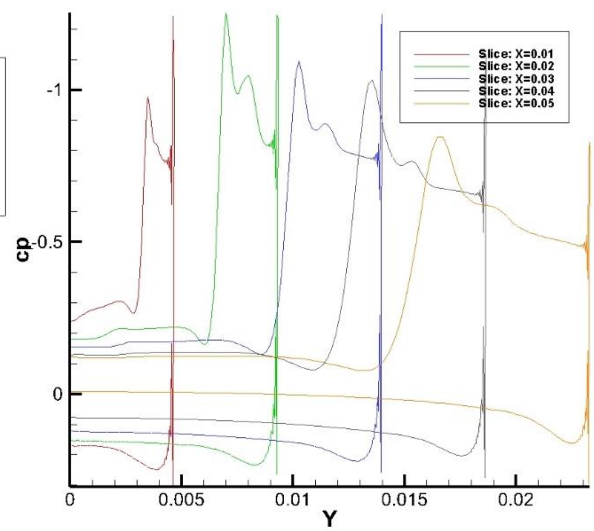

(b) SSG/LRR-ω model

Figure 6: Surface c_p Distribution for 65° sweep, α=10° (Y unit: m)

The Menter-SST model did achieve a stable vortex in a steady simulation, the model did not transport the vortex very well and the vortex was quickly dissipated. As seen in figure 7, the vortex from the Menter-SST model becomes weak very quickly, and that is undesirable for this study since we are mainly concerned with the vortex characteristics downstream of the wing.

Since the RSM-JHhv2 model could not resolve the flow, we decided to run simulations with the RSM-SSG/LRR-ω model. This model showed promise since the c_p distribution was much smoother as can be seen in figure 6. The model did not capture a discrete vortex, while the Menter-SST model and past research by Payne, Ng, Nelson, & Schiff (1988) showed a clear vortex for the flow. The flow characteristics were like an unsteady simulation, and thus the solver was switched to unsteady mode. The time step for the solver was set at $t_{conv}/200$, where the t_{conv}, the convective time step, is the the required for a particle to travel one chord length at freestream velocity ($t_{conv}=c_{\Delta}/U_{\infty}$). Under these conditions some sweep angles at certain angles of attack showed clear vortex. For other sweep angles and angles of attack, Karman vortices were seen at the trailing edge, and these Karman vortices interfered with the main vortex. Flow averaging over one convective time step was applied to filter out the influence of the Karman vortices. The difference between unaveraged and averaged results can be seen in figure 8. Table 2 shows the different cases that were simulated, and whether they needed flow averaging or not.

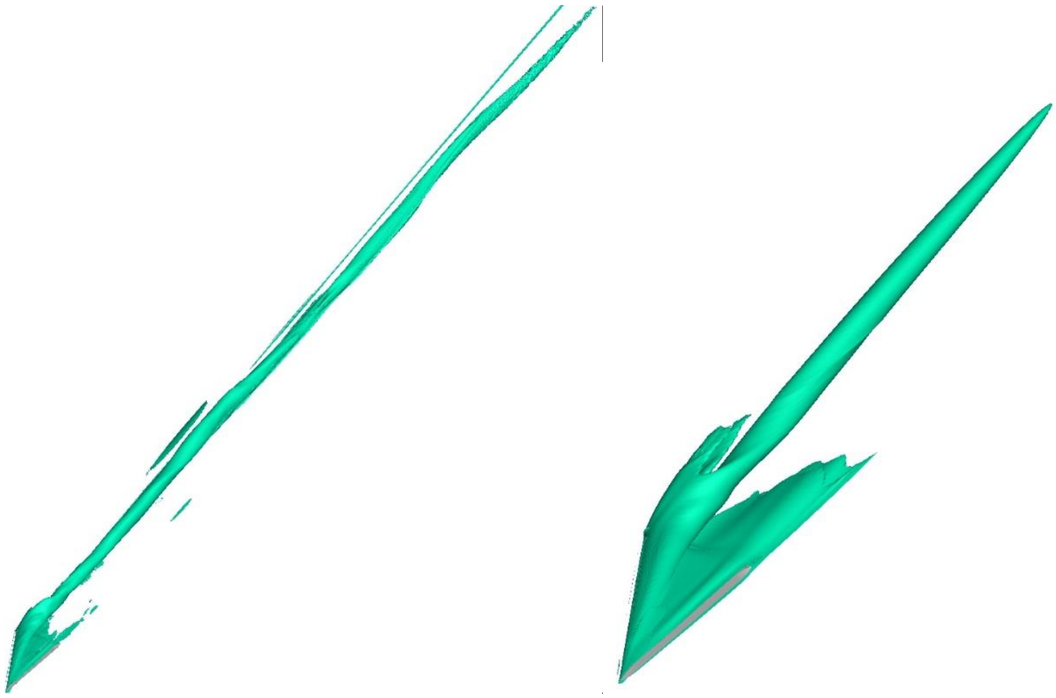

(a) RSM SSG/LRR-ω model (b) Menter-SST model

Figure 7: Difference between RSM and SST model simulations (65° sweep at α=10°, visualization of iso-surfaces at vorticity = 5000 s^{-1})

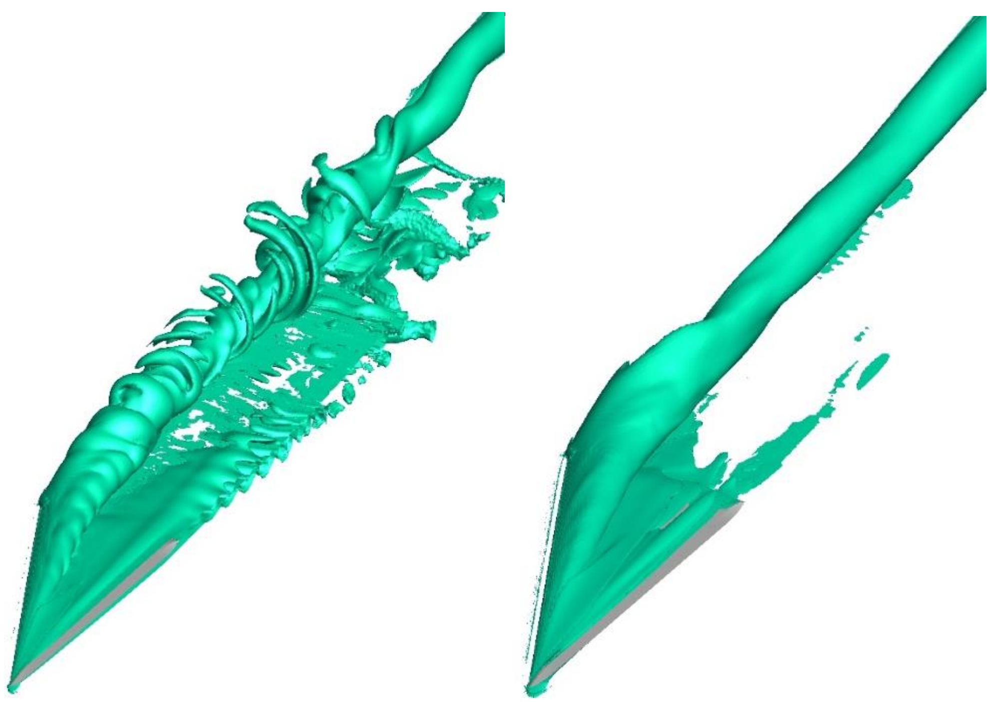

(a) Unaveraged flow (b) Averaged flow

Figure 8: Unaveraged vs Averaged vortex for 65° sweep at α=10° (Iso-surfaces at vorticity = 5000 s^{-1})

Table 2: Simulated Cases and Results

Angle of Attack (α)	Sweep Angle		
	65°	55°	45°
10°	Averaged over 1 t_{conv}	Unsteady-unaveraged simulation	
12.5°	Averaged over 1 t_{conv}		
15°	Averaged over 1 t_{conv}	Averaged over 0.1 t_{conv}	Averaged over 1 t_{conv} and 6 t_{conv}
17.5°	Averaged over 1 t_{conv}		
20°	Averaged over 1 t_{conv}	Averaged over 0.8 t_{conv}	

The cases for 55° sweep at α=15° and α=20° diverged. The α=15° case diverged in the 21st time step, though the earlier inner iterations converged. Similarly the α=20° case diverged at about 170 time steps. In order to promote convergence different parameters, including CFL number, time step and multi-grid, were changed to no avail. Though the accuracy of these simulations is questionable, since this study was for a fixed period, time constraints prevented us from getting a converged solution averaged over more time. From the analysis, it seems like the reason the simulations are diverging is that the time step is not small enough to resolve the Karman vortex street, and that causes the simulation to diverge. The other cases also take more iterations to converge for later time steps, showing that this phenomenon is not limited to these two cases.

The case of 45° sweep at α=15° showed unusually good convergence characteristics, and was therefore used as the case to compare averaging over one convective time step vs averaging over greater time (six convective time steps in this case). Comparing these two cases shows that to get a more accurate and reliable result, time averaging over a greater time would be required. Figure 9 shows the vortices resulting from the two cases, and the vortex averaged over six convective time steps is clearer.

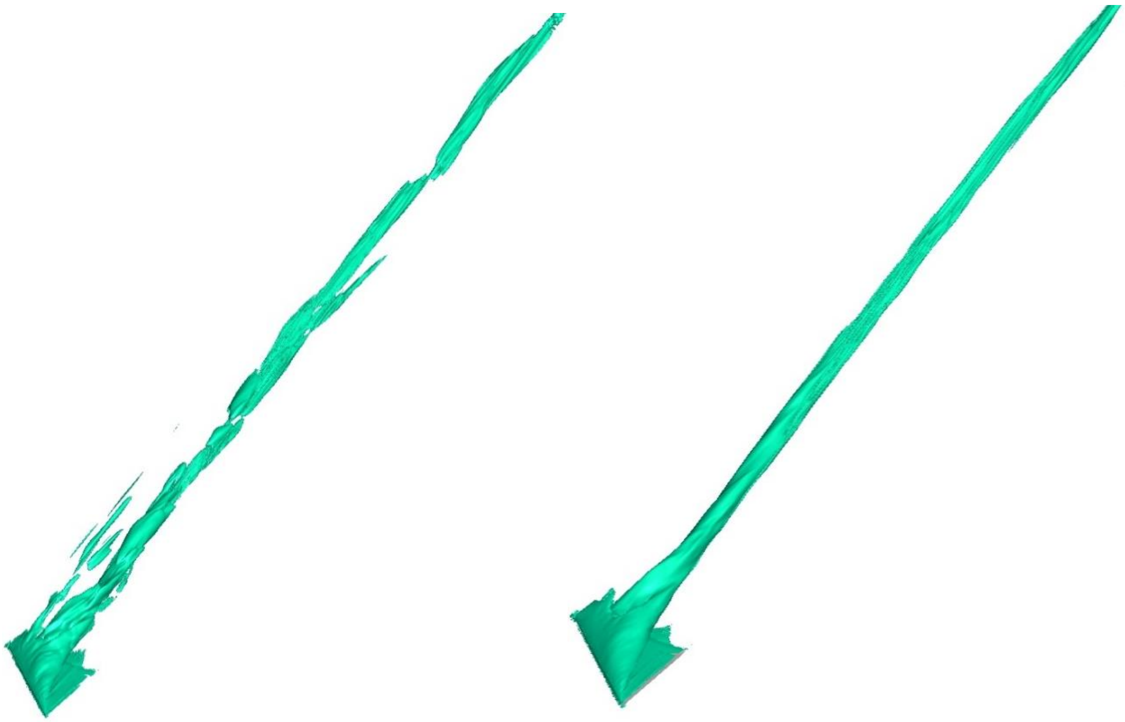

(a) Averaged over 1 t_{conv} (b) Averaged over 6 t_{tconv}

Figure 9: Effects of averaging over different amount of times (45° sweep α=15°, visualization of vortex using iso-surface at vorticity = 5000 s^{-1})

Some of the other cases also show the need for averaging over a longer time period since the mixing vortex can be seen separately in the vorticity views. Some examples are shown in figure 10. In figure 10 (a) and (b) there are multiple maxima for vorticity and it seems like there are multiple vortices rotating around a point. Figure 10 (c) and (d) also show unusual vorticity distribution which can be attributed to mixing of the longitudinal vortex with the Karman vortices.

Another observation from images in figure 10 is that some part of all of these vortices is in the unstructured region. All the vortices followed a lower angle to the wing than the freestream angle of attack. This was not foreseen and thus not accounted for. Due to the unstructured mesh being fine near the structured region, the vortex is not dissipated, but the solution is less accurate due to this. The vortices reached the unstructured region at about 4 chord lengths downstream from the trailing edge.

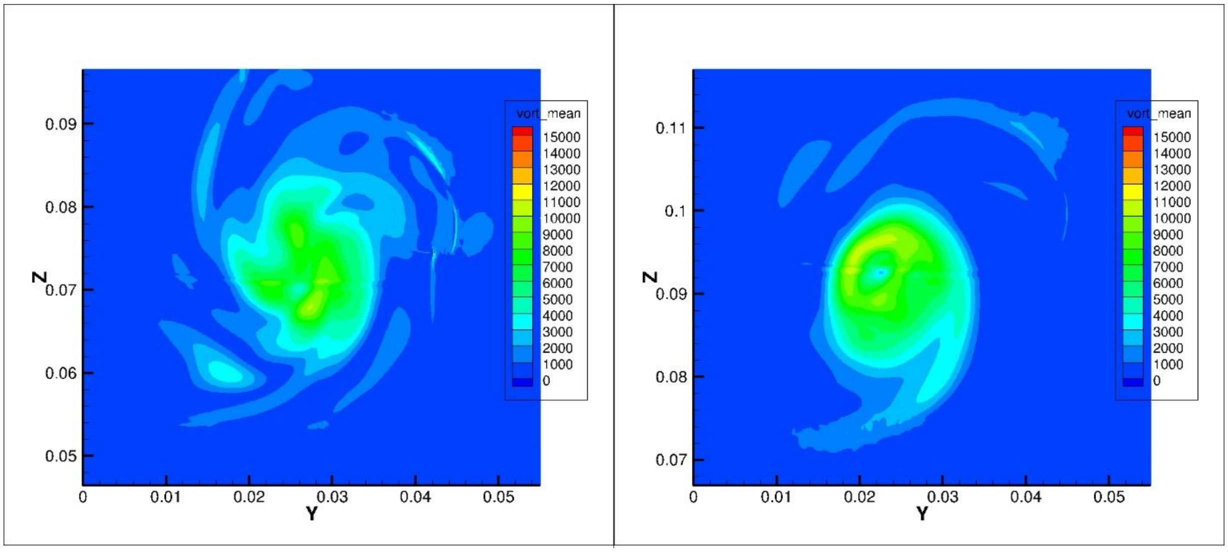

(a) 55° sweep α=20°, 4 chords downstream (b) 55° sweep α=20°, 5 chords downstream

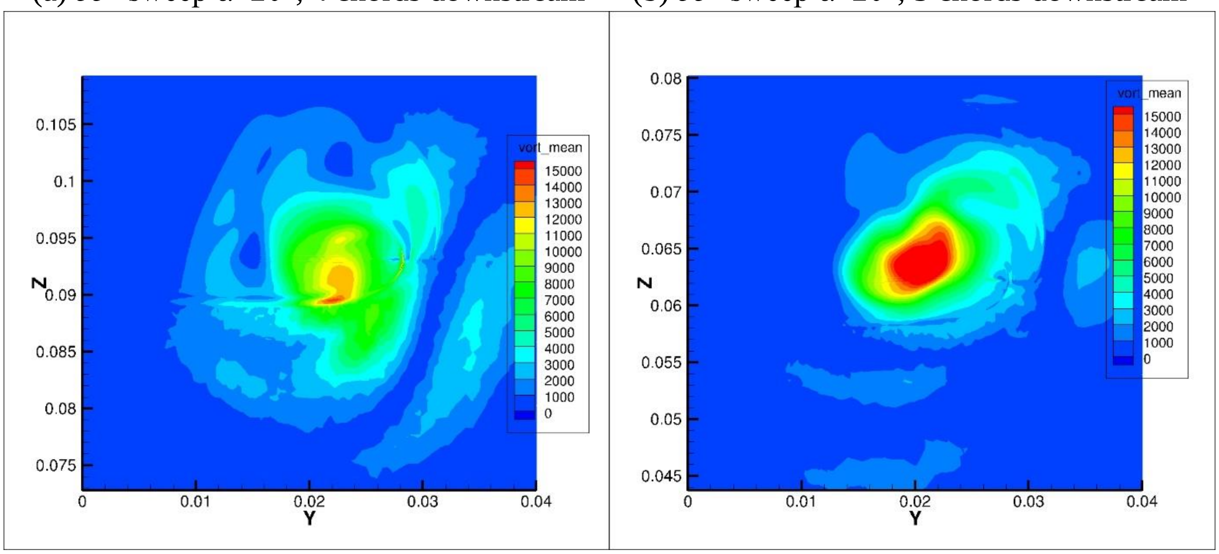

(c) 65° sweep α=20°, 5 chords downstream (d) 65° sweep α=17.5°, 4 chords downstream

Figure 10: Vorticity distribution (distances measured from trailing edge, vorticity unit: s^{-1})

Results and Discussion

Past data on flow over high-lift wings with strake vortices was analyzed by partners of the project from the DLR to determine the typical characteristics of a strake vortex. It was determined that the strake hits the main wing at 2-5 chord lengths downstream from the delta wing depending on the aircraft.

This analysis was used to determine the characteristics of a typical strake vortex which can be seen in table 3. This data along with results of this study will be used in the project to recreate a strake vortex in a numerical simulation and to validate the results of the simulation using a wind tunnel experiment. The parameters are discussed in more detail with the results of the simulations.

Table 3: Data for a typical Strake Vortex

Normalized Maximum Vorticity ($\omega_{max}*c_{main}/U_{\infty}$)	60
Normalized Circulation ($\Gamma/ c_{main}* U_{\infty}$)	0.1-0.2
Normalized Change in core velocity ($\Delta U/U_{\infty}$)	0.4
Normalized Diameter of vortex (d_{ω}/c_{main})	0.1-0.2

The longitudinal vortices generated by flow over the delta wing were evaluated on the parameters mentioned in table 3 above. The maximum vorticity (ω_{max}) is the maximum vorticity measured in the core of the vortex. The unit is s^{-1} and thus the value is non-dimensionalized as $\omega_{max}*c_{main}/U_{\infty}$ where c_{main} is the chord length of the main wing 0.6m. The variation of the normalized maximum vorticity with distance from the trailing edge can be seen in figure 11.

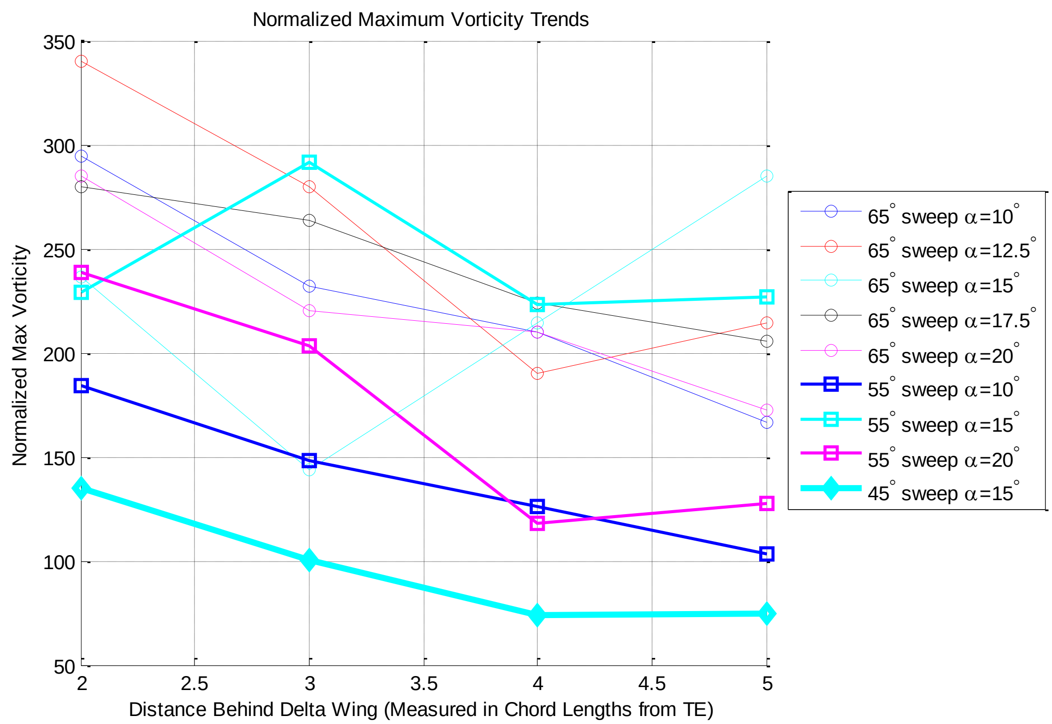

Figure 11: Normalized Max Vorticity vs Distance from Wing

Compared to a strake vortex, the maximum normalized vorticity is quite high for these simulations. The general trend as the vortex travels downstream is that the vorticity drops, as is expected. There are some anomalies probably caused by the mixing of Karman vortices. From figure 11, we can also notice that ω_{max} decreases with decreasing sweep angle and is not strongly affected by angle of attack.

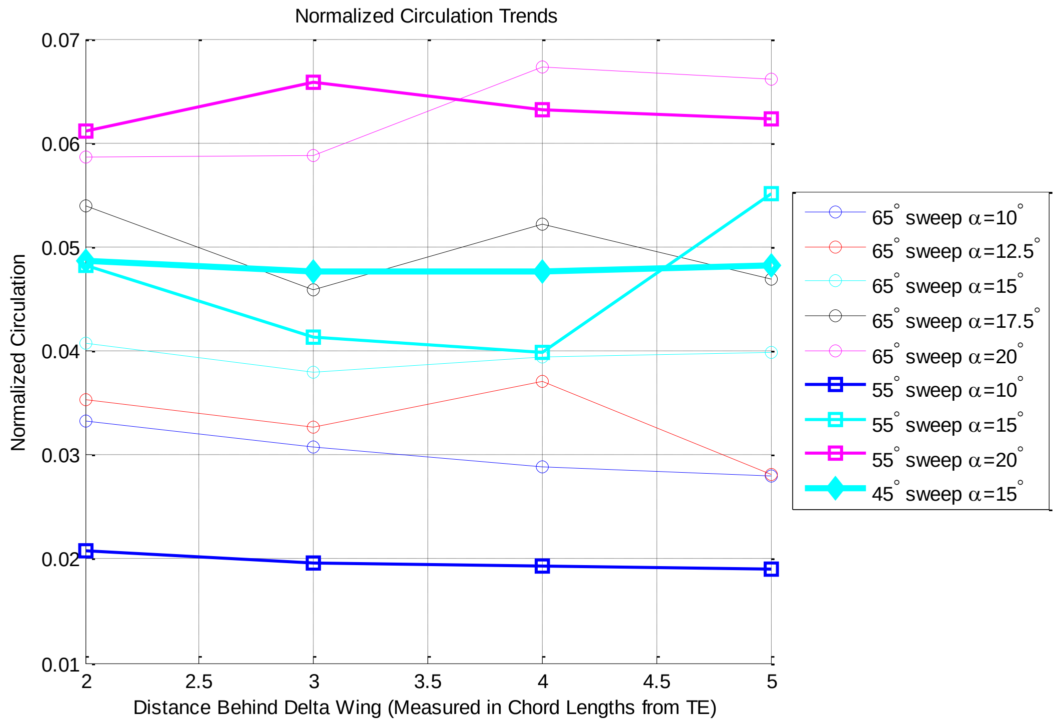

Figure 12: Normalized Circulation vs Distance behind Wing

Figure 12 shows the trends of normalized circulation with respect to the three variables, distance from wing, angle of attack and sweep angle. Circulation is calculated as the area integral of vorticity over the vortex. The mixing vortices make it difficult to define the boundary of the vortex leading to errors. The normalized circulation for all these vortices is smaller than the strake vortex. From figure 12 it can be inferred that circulation increases with sweep angle and angle of attack and does not vary greatly along the flow. In reality there would be a slight negative gradient of circulation with respect to distance along flow due to viscosity.

The case of 55° sweep at 10° angle of attack is an outlier to the trends noticed above since the circulation is smaller for this sweep angle than the circulation at 65° sweep and 10° angle of attack. This is probably because the 55° sweep at 10° angle of attack case was devoid of strong Karman vortices which probably increased the circulation of the other vortices.

Core velocity deficit is the difference between the freestream velocity and the velocity at the core of the vortex (at the point of max vorticity). In figure 13 we see how the core velocity deficit varies with the different variables. The core velocity deficit from the simulated vortices are close to those on a real strake. Anomalies in the values were caused due to multiple maxima at certain points, especially at 4 and 5 chord lengths downstream from the wing. From the plot the core velocity deficit looks unaffected by the sweep angle. It decreases with increasing distance from the wing, which is expected as the vortex dissipates. Though the relationship does not look very strong, velocity deficit increases with increasing angle of attack.

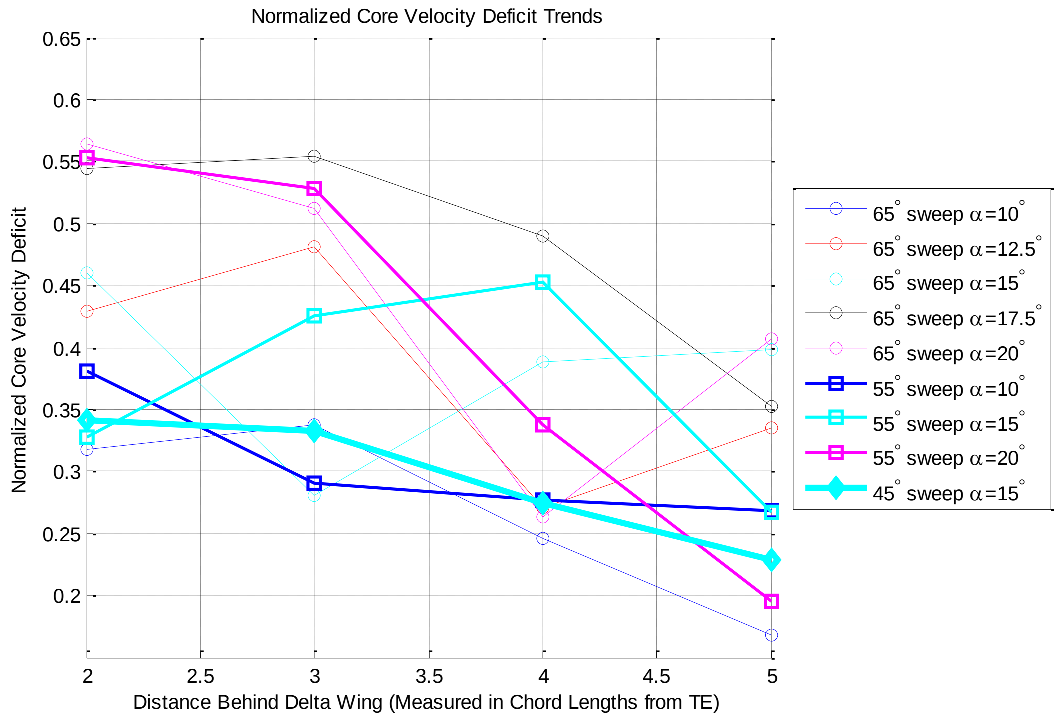

Figure 13: Normalized Core Velocity Deficit vs Distance from Wing

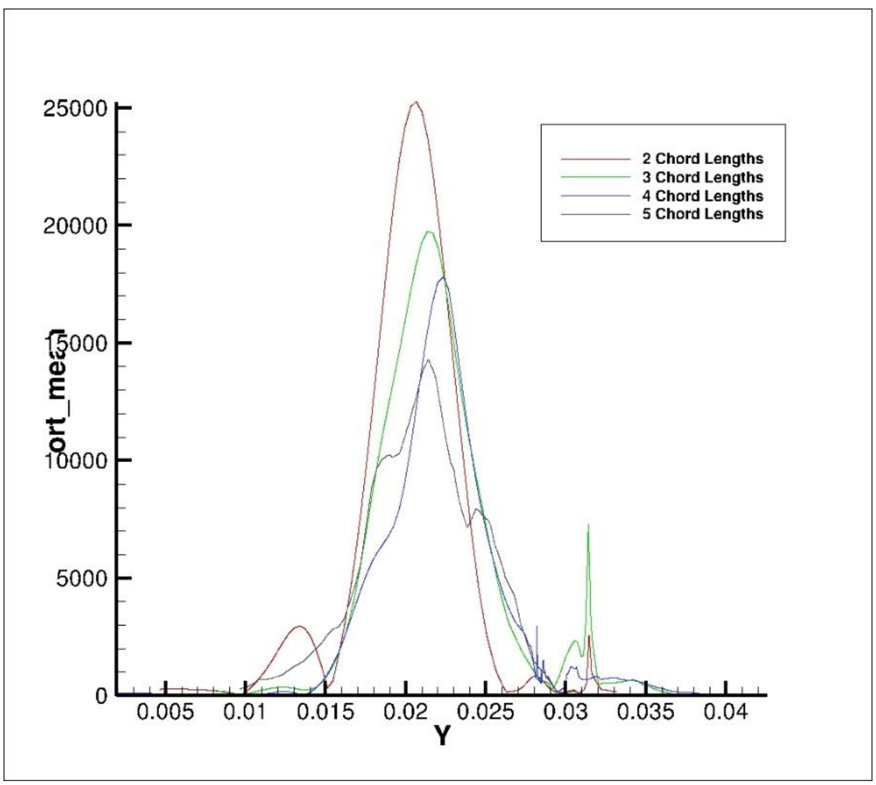

Figure 14: Vorticity distribution along horizontal line through core of vortex used to measure diameter. (x-axis unit: m, y-axis unit: s^{-1}; sweep angle 65°, α = 10°)

There are multiple methods to determine the diameter of the vortex. For this study, the diameter was measured from the vorticity distribution seen in figure 14. This distribution is obtained from a plane normal to the freestream by taking the distribution along a horizontal line passing through the core of the vortex. The diameter is the distance between the minimums on either side of the absolute maximum. The trends for this value can be seen in figure 15. The diameter of the vortex is also smaller than a strake vortex. Challenges in calculating this included multiple maxima, and oval shaped vortices which effectively had more than one diameter. The diameter of the vortex stays constant along the flow and increases with sweep angle and angle of attack. The fact that the diameter stays roughly constant along the flow can be verified from figure 14. This figure can also verify the observation that max vorticity decreases downstream.

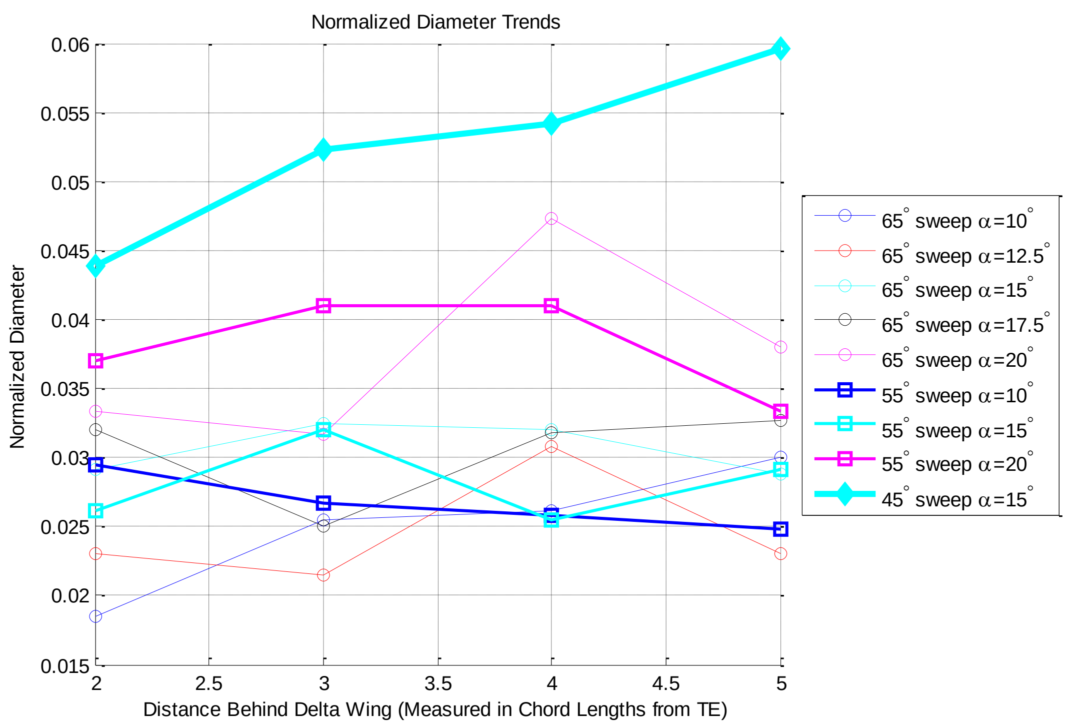

Figure 15: Normalized Diameter vs Distance from Wing

Since the Menter-SST model was used for verifying the grid resolution, we can use the data from that simulation to justify using RSM models. Figure 16 shows circulation vs distance from the wing computed from both the Menter-SST model and the RSM-SSG/LRR-ω model. Clearly the Menter-SST model does not capture the vortex as effectively.

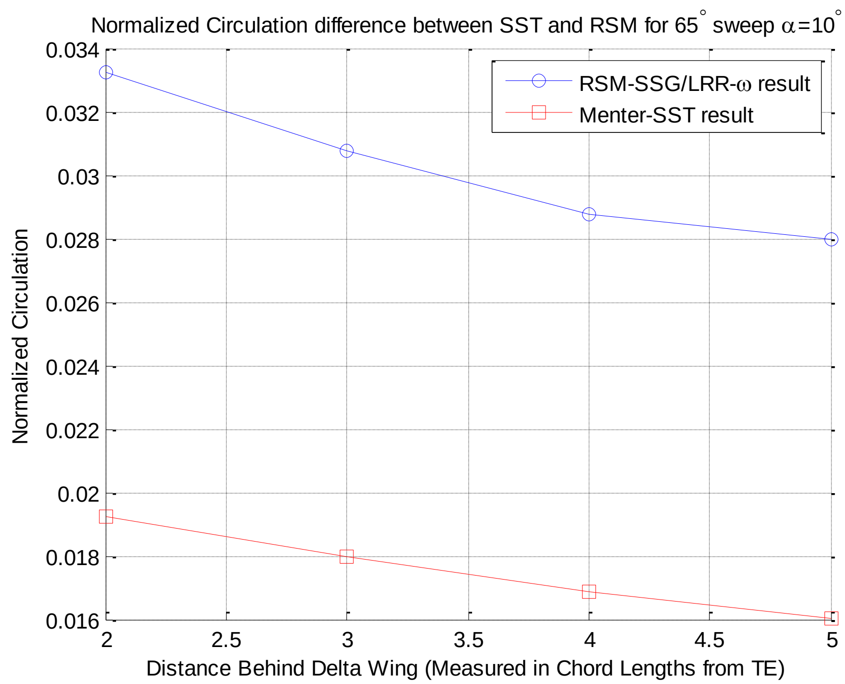

Figure 16: Circulation data from different turbulence models.

Table 4 summarizes all the trends mentioned in the analysis. The supervisor for this study, Tim Landa, reported from his study the effects of changing the chord length of the wing (thus changing the Reynolds number). This data can also be seen in the table.

Table 4: Trend followed by vortex characteristics with change in flow conditions.

Vortex Characteristics	**Flow Variables**			
	Distance from Wing	Angle of Attack	Sweep Angle	Chord Length
Max. Vorticity (ω_{max})	Decreases (↓)	Constant (−)	Decreases (↓)	Increases (↑)
Circulation (Γ)	Constant (−)	Increases (↑)	Increases (↑)	Increases (↑)
Core Velocity Defect ($\Delta U/U_\infty$)	Decreases (↓)	Increases (↑)	Constant (−)	Constant (−)
Diameter	Constant (−)	Increases (↑)	Increases (↑)	Increases (↑)

From the data it is clear that the vortices generated in this study are smaller than a strake vortex and the final experiment would need a larger delta wing to recreate a real strake vortex. Quantitative data on effects of size would be needed to determine the factor by which to scale up the wing.

Conclusion

Use of strake vortices has improved aircraft aerodynamics, but these devices still have to be designed through flight tests since there are no effective turbulence models to precisely model the vortices in numerical simulation. This study provides a starting point for the project that would delve into simulating a strake vortex. The trends provided here will help design the delta wing that would be the source of the strake vortex. Some of the trends can be verified with theory, like the fact that vorticity stays almost constant downstream of the flow agrees with Kelvin's circulation theorem.

Despite the best efforts, the study did face some problems that could not be solved given the time limited nature of the study. Two of these problems are mentioned here so future studies can avoid them. Firstly, the vortex seems to sink down, and therefore, a little distance downstream, moves into the unstructured region. This leads to grid interferences that affect the solution. While this can be tackled with a bigger structured region, this solution would be computationally expensive. Instead a small theoretical study can be conducted to determine how much the vortex would sink, and then the grid can be adjusted accordingly. The other problem was that combining the need for greater averaging, seen from the 45° sweep case, and smaller time steps, required for the 55° sweep 15° angle of attack case, would greatly increase the computational resources required. For future studies, there has to be a compromise reached between the two cases in order to get more accurate results with reasonable computational costs.

References

Rudnik, R., & Geyr, H. (2007). The European High Lift Project EUROLIFT II–Objectives, Approach, and Structure. *AIAA Paper*, *4296*, 2007.

Menter, F. R. (1993). Zonal two equation k-turbulence models for aerodynamic flows. *AIAA paper*, *2906*, 1993.

Cécora, R. D., Eisfeld, B., Probst, A., Crippa, S., & Radespiel, R. (2012, January). Differential reynolds stress modeling for aeronautics. In *50th AIAA Aerospace Sciences Meeting* (Vol. 465).

Subbian, G. (2016, March). Vortical Flow Simulation with an Eddy Viscosity Model of Turbulence. *Master's thesis at Institut für Strömungsmechanik, Technische Universität Braunschweig.*

Earnshaw, P. B., & Lawford, J. A. (1966). *Low-speed wind-tunnel experiments on a series of sharp-edged delta wings*. HM Stationery Office.

Payne, F. M., Ng, T., Nelson, R. C., & Schiff, L. B. (1988). Visualization and wake surveys of vortical flow over a delta wing. *AIAA journal*, *26*(2), 137-143.

Appendix

```
--------------------------------------------------
PREPROCESSING
--------------------------------------------------
   Files/IO --------------------------------------: -
                       Boundary mapping filename: Para_files/bmap.para
                           Primary grid filename: Grid_files/DeltaWing65_10deg.grd
                                     Grid prefix: Dualgrid_files/dualgrid
                                   Output format: tecplot
   Logfile control -------------------------------: -
         Enable logfile output on all domains (0/1): 0
   Parameter -------------------------------------: -
                       Number of multigrid levels: 4
                                     Output level: 20
   Runtime optimisation --------------------------: -
                     Bandwidth optimisation (0/1): 1
                      Compute lusgs mapping (0/1): 1
              2D offset vector (0 / x=1, y=2, z=3): 0
 Extras ---------------------------------------: -
                       Compute exact surface(0/1): 1
 Partitioning ----------------------------------: -
                     Type of partitioning (name): private
                               Number of domains: 720
                   Number of primary grid domains: 720
 --------------------------------------------------
 SOLVER
 --------------------------------------------------
   Files/IO --------------------------------------: -
                             Restart-data prefix: (none)
                             Output files prefix: Solution_files/solution_10deg
                Automatic parameter update (0/1): 1
   Timestepping Start/Stop -----------------------: -
                                   Output period: 20000
                         Maximal time step number: 40000
   Monitoring ------------------------------------: -
                           Monitor history (0/1): 1
                               Monitoring values: Residual_dr11/dt_deps-rsm/dt_C-lift_C-drag_C-
my_X-max-res_Y-max-res_Z-max-res_Max-res_Max-y+_Max-eddyv
   Memory management -----------------------------: -
                           Increase memory (0/1): 1
   Transport coefficients ------------------------: -
                                 Reynolds number: 2.0e5
                                  Prandtl number: 0.72
                             Sutherland constant: 110.4
                  Sutherland reference viscosity: 1.716e-05
                Sutherland reference temperature: 273
                           Reference temperature: 293.15
                                 Reynolds length: 0.06
                           Reference Mach number: 0.15
   Geometry --------------------------------------: -
                                      Grid scale: 1
                         Reference relation area: 0
             Reference length (pitching momentum): 1
       Reference length (rolling/yawing momentum): 1
                            Origin coordinate x: 0
                            Origin coordinate y: 0
                            Origin coordinate z: 0
   Flux ------------------------------------------: -
               Inviscid flux discretization type: Central
                       Central dissipation scheme: Scalar_dissipation               #
Matrix_dissipation
                 Central convective meanflow flux: Average_of_flux
                Central convective turbulence flux: Roe
```

```
                 | 2nd order dissipation coefficient: 0.5
        Inverse 4th order dissipation coefficient: 64
    Relaxation ---------------------------------------: -
                                 Relaxation solver: Backward_Euler #Runge_Kutta
    Backward Euler ----------------------------------: -
                                     Linear solver: Lusgs
                       Implicit overrelaxation omega: 1
        LUSGS ---------------------------------------: -
         Lusgs increased parallel communication (0/1): 1
    Multigrid ---------------------------------------: -
                           MG description filename: 3w++
                        SG start up steps (fine grid): 1000
                             MG source terms (0/1): 1
                           Multigrid indicator (0/1): 1
      Full multigrid ---------------------------------: -
                               Multigrid start level: 1
                Maximal time step number (coarse grids): 1000
                       Minimum residual (coarse grids): 0.0001
        Full multigrid central scheme first-order (0/1): 0

    Timestepsize ------------------------------------: -
                                         CFL number: 1
                         #CFL number (coarse grids): 1.3
                         #CFL number (large grad p): 1.3
                          Viscous time step factor: 0.25
                         Time step smoothing factor: 2

     Turbulence --------------------------------------: -
                          Turbulence model version: RSM
                            Ratio Prandtl lam/turb: 0.8
                         General ratio mue-t/mue-l: 0.1
                       General turbulent intensity: 0.001
                          Reference bl-thickness: 0.1
             Turbulence equations use multigrid (0/1): 0

    RSM ---------------------------------------------: -
                         Rsm re-distribution model: SSG/LRR-w.2010
                        Rsm implementation version: FLOWer
                             Rsm dissipation model: isotropic
                               Rsm diffusion model: GGDH.2010
                         Rsm length scale equation: Menter_BSL_omega


     Preconditioning ---------------------------------: -
                                  Preconditioning: PrimNew  #none used for some simulations
                                     Cut-off value: 4

         Cauchy convergence control -----------------: -
                    Use Cauchy convergence control: relative
              Cauchy convergence control variables: C-lift_C-drag_C-my_Max-y+_Max-eddyv
              Error for Cauchy convergence control: 1e-6 1e-6 1e-6 1e-6 1e-6
           Number of samples for Cauchy convergence: 20
              Factor for dynamic Cauchy convergence: 0.05

     Dual time ---------------------------------------: -
                            Unsteady time stepping: dual
        Unsteady activate inner iteration output (0/1): 0
                 Unsteady show pseudo time steps (0/1): 1
                      Unsteady physical time step size: 0.0000058275 #=1/200 konv. TS, 1 Konvektiver
Zeitschritt = 0.01167
                          Unsteady physical time steps: 40
               Unsteady inner iterations per time step: 1000
```

```
                    Unsteady implicit scheme order: 2
                     Unsteady extrapolation order: 0
      Compute harmonics of global forces (0/1..n): 0
           Compute harmonics on surface (0/1): 0

   Flow time averaging ------------------------------: -
                         Compute flow statistics: mean_variance_meanvelgrad
                           Reset flow statistics: (none) #mean_variance_meanvelgrad

 -----------------------------------------------------
 Surface output
 -----------------------------------------------------
                  Surface output description file: (thisfile)
                            Surface output values: xyz_rho_cp_cf_yplus_cfxyz_rotcorr #_mean-
cp_mean-cf
                            Surface output period: 20000
 -----------------------------------------------------
 cut plane output
 -----------------------------------------------------
                                 Number of planes: 3
                                   Plane normal x: 1
                                   Plane normal y: 0
                                   Plane normal z: 0
                              Plane output period: 20 20 20
                                  Plane support x: 0.06 0.18 0.36
                                  Plane support y: 0 0 0
                                  Plane support z: 0 0 0
                              Plane output values: cp_v
 -----------------------------------------------------
 Extra field pointdata output
 -----------------------------------------------------
                    Field output description file: (thisfile)
                              Field output values: cp_mach_muetmue_wdist_Rrho_Q_vort
#_mean_variance
 -----------------------------------------------------
 -----------------------------------------------------
 Updates
 -----------------------------------------------------
```